REPORT DOCUMENTATION PAGE

Form Approved OMB NO. 0704-0188

1. REPORT DATE (DD-MM-YYYY)	2. REPORT TYPE	3. DATES COVERED (From - To)
24-11-2015	Final Report	20-Jul-2014 - 19-Jul-2015

4. TITLE AND SUBTITLE

Final Report: Instruments for Characterizing Carbon and Sulfur-Resistant Core-Shell Redox Catalysts for Combined Hydrocarbon Reforming and Water-Splitting

5a. CONTRACT NUMBER
W911NF-14-1-0362

5b. GRANT NUMBER

5c. PROGRAM ELEMENT NUMBER
611102

6. AUTHORS

Fanxing Li

5d. PROJECT NUMBER

5e. TASK NUMBER

5f. WORK UNIT NUMBER

7. PERFORMING ORGANIZATION NAMES AND ADDRESSES

North Carolina State University
2701 Sullivan Drive
Admin Services III; Box 7514
Raleigh, NC 27695 -7514

8. PERFORMING ORGANIZATION REPORT NUMBER

9. SPONSORING/MONITORING AGENCY NAME(S) AND ADDRESS (ES)

U.S. Army Research Office
P.O. Box 12211
Research Triangle Park, NC 27709-2211

10. SPONSOR/MONITOR'S ACRONYM(S)
ARO

11. SPONSOR/MONITOR'S REPORT NUMBER(S)
65260-CH-RIP.7

12. DISTRIBUTION AVAILIBILITY STATEMENT

Approved for Public Release; Distribution Unlimited

13. SUPPLEMENTARY NOTES

The views, opinions and/or findings contained in this report are those of the author(s) and should not contrued as an official Department of the Army position, policy or decision, unless so designated by other documentation.

14. ABSTRACT

This project aims to investigate a novel core-shell redox catalyst for combined methane partial oxidation and water-splitting. The effect of support, mechanism, and novel applications of perovskite supported iron oxide as a versatile redox catalyst are investigated. Properly designed redox catalyst are shown to be highly effective for syngas production (from methane) and water-splitting. The resulting syngas has a composition readily usable for Fischer-Tropsch synthesis whereas the hydrogen generated is of high purity. In addition, coke formation can be avoided if the redox catalyst is regenerated before complete reduction of iron oxide into metallic iron. High syngas selectivity

15. SUBJECT TERMS

redox catalyst, methane partial oxidation, water-splitting

16. SECURITY CLASSIFICATION OF:			17. LIMITATION OF ABSTRACT	15. NUMBER OF PAGES	19a. NAME OF RESPONSIBLE PERSON
a. REPORT	b. ABSTRACT	c. THIS PAGE			Fanxing Li
UU	UU	UU	UU		19b. TELEPHONE NUMBER 919-515-7328

Report Title

Final Report: Instruments for Characterizing Carbon and Sulfur-Resistant Core-Shell Redox Catalysts for Combined Hydrocarbon Reforming and Water-Splitting

ABSTRACT

This project aims to investigate a novel core-shell redox catalyst for combined methane partial oxidation and water-splitting. The effect of support, mechanism, and novel applications of perovskite supported iron oxide as a versatile redox catalyst are investigated. Properly designed redox catalyst are shown to be highly effective for syngas production (from methane) and water-splitting. The resulting syngas has a composition readily usable for Fischer-Tropsch synthesis whereas the hydrogen generated is of high purity. In addition, coke formation can be avoided if the redox catalyst is regenerated before complete reduction of iron oxide into metallic iron. High syngas selectivity, steam to hydrogen conversion, and inhibition of coke formation are observed in the current study.

Enter List of papers submitted or published that acknowledge ARO support from the start of the project to the date of this printing. List the papers, including journal references, in the following categories:

(a) Papers published in peer-reviewed journals (N/A for none)

Received		Paper
11/22/2015	1.00	Luke M. Neal, Arya Shafiefarhood, Fanxing Li. Dynamic Methane Partial Oxidation Using a Fe2O3@La0. 8Sr0.2FeO3-? Core–Shell Redox Catalyst in the Absence of Gaseous Oxygen, ACS Catalysis, (10 2014): 0. doi: 10.1021/cs5008415
11/22/2015	2.00	Luke Neal, Arya Shafiefarhood, Fanxing Li. Effect of core and shell compositions on MeOx@LaySr1? yFeO3 core–shell redox catalysts for chemical looping reforming of methane, Applied Energy, (11 2015): 0. doi: 10.1016/j.apenergy.2015.06.028
11/22/2015	3.00	Feng He, Fanxing Li. Hydrogen production from methane and solar energy – Process evaluations and comparison studies, International Journal of Hydrogen Energy, (10 2014): 0. doi: 10.1016/j.ijhydene.2014.05.089
11/22/2015	4.00	Feng He, Fanxing Li. Perovskite promoted iron oxide for hybrid water-splitting and syngas generation with exceptional conversion, Energy Environ. Sci., (12 2015): 0. doi: 10.1039/C4EE03431G
11/22/2015	5.00	Arya Shafiefarhood, Joseph Clay Hamill, Luke Michael Neal, Fanxing Li. Methane partial oxidation using FeO, Phys. Chem. Chem. Phys., (11 2015): 0. doi: 10.1039/C5CP05583K
11/22/2015	6.00	Yanguang Chen, Nathan Galinsky, Ziren Wang, Fanxing Li. Investigation of perovskite supported composite oxides for chemical looping conversion of syngas, Fuel, (10 2014): 0. doi: 10.1016/j.fuel.2014.06.017
TOTAL:	**6**	

Number of Papers published in peer-reviewed journals:

(b) Papers published in non-peer-reviewed journals (N/A for none)

Received Paper

TOTAL:

Number of Papers published in non peer-reviewed journals:

(c) Presentations

Number of Presentations: 0.00

Non Peer-Reviewed Conference Proceeding publications (other than abstracts):

Received Paper

TOTAL:

Number of Non Peer-Reviewed Conference Proceeding publications (other than abstracts):

Peer-Reviewed Conference Proceeding publications (other than abstracts):

Received Paper

TOTAL:

Number of Peer-Reviewed Conference Proceeding publications (other than abstracts):

(d) Manuscripts

Received Paper

TOTAL:

Number of Manuscripts:

Books

Received Book

TOTAL:

Received Book Chapter

TOTAL:

Patents Submitted

Patents Awarded

Awards

The PI received the following awards resulting from his research activities (partially supported by ARO DURIP):
Sigma Xi Faculty Research Award at NC State University, 2015
SABIC Young Professional Award of the Particle Technology Forum of AIChE, 2015
University Faculty Scholar at NC State University, 2015

Graduate Students

NAME	PERCENT_SUPPORTED	Discipline
Arya Shafiefarhood	0.00	
Nathan Galinsky	0.00	
Feng He	0.00	
FTE Equivalent:	**0.00**	
Total Number:	**3**	

Names of Post Doctorates

NAME	PERCENT_SUPPORTED
Luke Neal	0.00
FTE Equivalent:	**0.00**
Total Number:	**1**

Names of Faculty Supported

NAME	PERCENT_SUPPORTED	National Academy Member
Fanxing Li	0.00	
FTE Equivalent:	**0.00**	
Total Number:	**1**	

Names of Under Graduate students supported

NAME	PERCENT_SUPPORTED
FTE Equivalent:	
Total Number:	

Student Metrics

This section only applies to graduating undergraduates supported by this agreement in this reporting period

The number of undergraduates funded by this agreement who graduated during this period: 0.00

The number of undergraduates funded by this agreement who graduated during this period with a degree in science, mathematics, engineering, or technology fields:..... 0.00

The number of undergraduates funded by your agreement who graduated during this period and will continue to pursue a graduate or Ph.D. degree in science, mathematics, engineering, or technology fields:..... 0.00

Number of graduating undergraduates who achieved a 3.5 GPA to 4.0 (4.0 max scale):..... 0.00

Number of graduating undergraduates funded by a DoD funded Center of Excellence grant for Education, Research and Engineering:..... 0.00

The number of undergraduates funded by your agreement who graduated during this period and intend to work for the Department of Defense 0.00

The number of undergraduates funded by your agreement who graduated during this period and will receive scholarships or fellowships for further studies in science, mathematics, engineering or technology fields:..... 0.00

Names of Personnel receiving masters degrees

NAME
Total Number:

Names of personnel receiving PHDs

NAME
Feng he
Total Number: 1

Names of other research staff

NAME	PERCENT_SUPPORTED
FTE Equivalent:	
Total Number:	

Sub Contractors (DD882)

Inventions (DD882)

Scientific Progress

see attachment

Technology Transfer

Final Technical Report for: Instruments for Characterizing Carbon and Sulfur-Resistant Core-Shell Redox Catalyst for Combined Hydrocarbon Reforming and Water-Splitting

W911NF-14-1-0362

Equipment Purchased Resulting from the Grant

No.	Instrument	Manufacturer	Purchase Price
1	ASAP 2020C	Micromeritics	$58,277.12
2	XPS Pre-treatment Chamber	Fabricated equipment form multiple vendors: Vat Inc., Duniway Stockroom Corp, Pfeiffer Vacuum.	$26,771.58
3	MB-10 Purifier	M Braun	$ 11,692.30
4	Paar XRK 900 - Z AXIS Stage	PANalytical	$ 27,000.00
5	7890B Fast RGA Gas Chromatography	Agilent/Restek, Swagelok North Carolina	$ 64,300.72

Five instruments were assembled (XPS Pre-treatment Chamber) or purchased in whole (ASAP 2020C BET/ Chemisorption instrument, a 7890B Fast RGA gas chromatograph, MB-10 purifier) or in part (PANalytical Paar XRK 900 - Z AXIS Stage) resulting from the ARO grant. All instruments are (and will be) used for catalyst activity and material characterization studies of core-shell redox catalyst and hydrocarbon reforming. The PANalytrcal stage was purchased in collaboration with AIF to take full advantage of the Empyrean XRD system by allowing insulted measurements of core-shell redox catalyst for reforming and water splitting. These new instruments have significantly expanded the research capabilities at the PI's lab and NCSU. The instruments have been used for graduate and undergraduate student research projects.

The purchase of these instruments was made October 2015 to January 2015 except for the GC that was purchased in July 2015. The time for purchases of the equipment was consistent with needs for updated quotes, approval purchase orders, sole-source justifications, and verification state-mandated NRTL (e.g. UL) certification. Leveraging the capabilities of existing XPS system, for the treatment chamber design allowed the purchase a GC for the characterization of redox catalyst activity, and was put to immediate use in the study of low temperature hydrocarbon reforming.

The PI's research group made significant progress in the study of redox reforming catalyst. The instruments are being used to assist the PI's research. During the project period, several very

promising catalysts were developed and characterized. This has led to five peer-reviewed articles in leading journals within the field. Technical details related to the project are described below:

Statement of the problem

Our previous findings shows that use of mixed ionic electronic conductors such as $La_xSr_{1-x}FeO_3$ can significantly enhance the performance of metal oxides such as iron oxide in chemical looping systems. We also reported successful synthesis of core-shell structure Fe_2O_3@LSF via a sol-gel based sequential synthesis approach. Compared to other iron-based composite redox catalysts such as those supported with $MgAl_2O_4$, Al_2O_3, Yttria-Stabilized-Zirconia (YSZ), and $La_xSr_{1-x}FeO_3$, the core-shell redox catalyst is up to 200 times more reactive. The catalyst is also selective towards syngas formation while showing satisfactory resistance towards coke formation.

The research project in this period is followed a number of directions in connection with the previous findings. A great deal of research is devoted to investigating the underlying mechanisms of methane partial oxidation using Fe_2O_3:LSF system. The core-shell Fe_2O_3@LSF, composite Fe_2O_3:LSF, and single-phase LSF based redox catalysts are characterized in detail in order to obtain mechanistic insights for the improved redox performance. The core-shell redox catalyst is found to be highly effective for syngas production. X-ray photoelectron spectroscopy (XPS) measurements indicate stable surface coverage of perovskites for the core-shell redox catalyst over 50 redox cycles. Further investigation of methane-redox catalyst reactions reveals a highly dynamic reaction scheme that can be divided into four regions, i.e. (i) a deep methane oxidation region attributable to loosely bonded lattice oxygen in addition to surface oxygen species; (ii) a competing deep and selective oxidation region attributable to relatively high surface oxygen coverage and abundant bulk lattice oxygen supply; (iii) a selective oxidation region with auto-activation attributable to reduced surface iron species and tightly bonded lattice oxygen species; and (iv) a methane decomposition and coke formation region resulting from O^{2-} depletion. Until region iv, the catalyst show minimal coke formation. This indicates that coke formation can be completely avoided with timely regeneration of the redox catalyst.

Furthermore, as confirmed by isotope exchange, the core-shell catalyst in these regions demonstrated markedly different mechanisms. While oxygen evolution maintains a modified Mars-van Krevlen mechanism throughout the reaction with O^{2-} conduction being the rate limiting step, the mechanism of methane conversion changes from an Eley-Rideal type in the first reaction region to a Langmuir-Hinshelwood-like mechanism in the third region.

The FeO_x:LSF composite system is also tested in a novel and highly effective hybrid solar-redox scheme for methane partial oxidation and water-splitting. In contrast to previously reported ferrite materials, which typically exhibit 20% or lower steam to hydrogen conversion, $La_{0.8}Sr_{0.2}FeO_{3-\delta}$ (LSF) promoted Fe_3O_4 is capable of converting more than 67% steam with high redox stability. Both experiments and a defect model indicate that the synergistic effect of reduced LSF and metallic iron phases is attributable to the exceptional steam conversion. To further enhance such a synergistic effect, a layered reverse-flow

reactor concept is proposed. Using this concept, over 77% steam to hydrogen conversion is achieved at 930 °C, which is 15% higher than the maximum conversion predicted by second law for unpromoted iron (oxides). When applied to the hybrid solar-redox scheme for liquid fuels and hydrogen co-generation, significant improvements in energy conversion efficiency can be achieved with reduced CO_2 emissions.

Besides the abovementioned efforts, we have also investigated low cost perovskite materials as potential support for iron oxide and their application in cyclic redox processes. As can be seen, the DURIP grant has, in part, allowed us to explore the fundamental mechanism of the core-shell redox catalyst concept and demonstrate its versatility for a number of applications for F-T ready syngas production and H2 generation.

Summary of results

1. Dynamic methane partial oxidation using a $Fe_2O_3@La_{0.8}Sr_{0.2}FeO_{3-\delta}$ core-shell redox catalyst

Catalyst preparation, characterization, and redox testing

Catalysts are prepared by a sol-gel modified Pechini method described in previous work.[1] Reactivity studies are conducted in a SETARAM SETSYS Evolution Thermal Gravimetric Analyzer (TGA). Redox experiments are performed at 900 °C. The reduction and oxidation steps are performed in 10% methane balance helium and 10% oxygen balance helium, respectively. The products for the reduction and oxidation steps are monitored using a quadruple mass spectrometer (QMS, MKS Cirrus II). The products are calculated by integrating the signals for the characteristic peaks of each species.

For measurements such as temperature programmed desorption and pulse reaction, a U-tube reactor is used to reduce rector dead volume and to minimize back mixing. U-tube reactor tests are performed with 200mg of sample in a ¼" O.D. quartz U-tube and heated by a tube furnace. A mass flow controller (MFC) valve manifold is used to pre-treat the sample in the desired atmosphere. The products from the reactor are measured with the QMS.

X-ray photoelectron spectroscopy (XPS) is used to probe the near-surface composition of the fresh, 10-cycle, and 50-cycle catalysts. The system is comprised of a Thermo-Fisher Alpha 110 hemispherical energy analyzer, a Thermo-Fisher XR3, 300 watt duel anode x-ray source, and a chamber with a base pressure of 1×10^{-9} Torr. Mg anode is used. Survey spectra are taken with pass energy of 100 eV, and narrow scan spectra are taken with pass energy of 20 eV. The XPS spectra indicate that the LSF phase at the catalyst surface is relatively stable over 50 redox cycles. They also indicate a reasonable LSF coating of the iron nanoparticles.

Powder X-ray diffraction (XRD) is carried out to analyze the crystal phase composition before and after cycling using a Rigaku SmartLab X-ray diffractometer. A continuous scan with a 0.02 ° resolution is used

to collect the patterns. The patterns are processed in Hi-Score Plus. The BET surface areas are characterized using a Micromeritrics Gemini VII 2390a via a 7 point physisorption measurement at 77.3 K with nitrogen as adsorbate. Prior to testing, the samples are outgassed for 30 minutes at 200°C.

Mechanism study on dynamic methane partial oxidation

Figure 1 shows a time-dependent product profile from a typical reduction cycle of the core-shell redox catalyst. As can be seen, the reduction of the core-shell catalyst can be divided into four distinct regions based on syngas yield and selectivity: (i) an initial region dominated by deep oxidation; (ii) a transition region of competing deep and selective oxidation; (iii) a selective oxidation region of increasing activity; and (iv) a coking region dominated by methane decomposition.

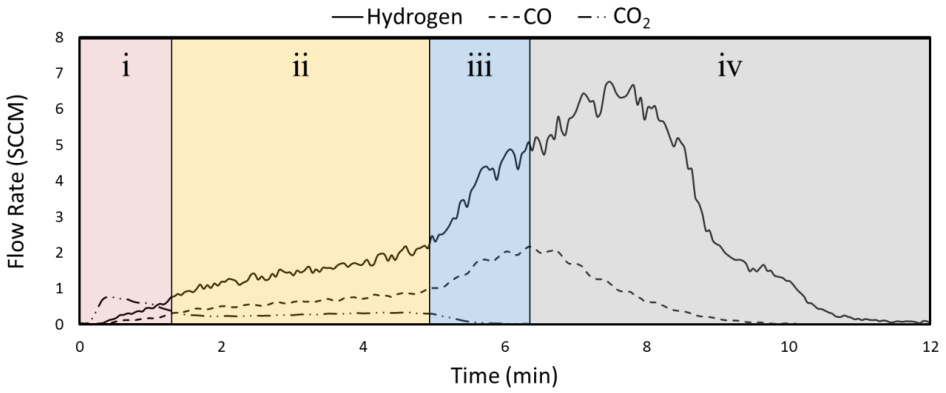

Figure 1. Temporal yields of gaseous products during the reduction of Fe_2O_3@LSF with methane

Figure 2 compares weight loss of the core-shell catalyst calculated from experimental data and the corresponding phases from theoretical prediction (based on thermodynamic data from HSC). As can be seen, region i-ii and iii-iv transitions appear to correlate with the average oxidation state of iron in the core. The demarcation of regions i and ii aligns with the depletion of hematite to Fe_3O_4. The highly selective region iii corresponds to a co-existence of metallic iron and wustite phases. The transition from region iii to iv roughly corresponds to the predicted depletion of oxygen from the iron phase. Thus, decomposition of LSF is likely to occur in region iv. The corresponding precipitation of metallic iron that occurs during LSF decomposition would catalyze methane decomposition and coke formation. The higher propensity of the composite sample to coke vs pure LSF indicates that higher availability of metallic iron may lead to increased coke formation.

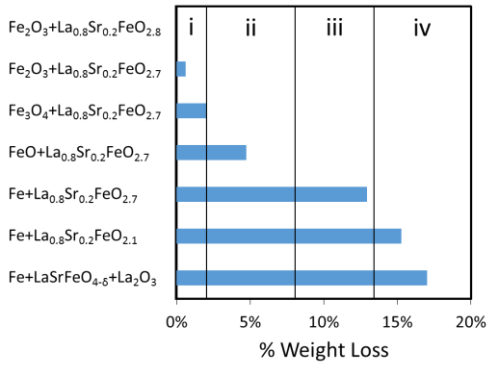

Figure 2. Core-shell redox catalyst weight loss for the four regions and corresponding phases calculated based on thermodynamic prediction of average oxidation states

To obtain a better understanding of the underlying mechanisms causing such selectivity shifts, transient pulse injection experiments are conducted on the core-shell redox catalyst in Regions i and iii. The following experiments are designed to probe the amount and nature of the non-selective surface oxygen species, through: i) examination of product responses in consecutive pulses; ii) increasing the bulk lattice oxygen supply (increasing the relaxation time); iii) co-feeding gaseous oxygen and monitoring its effects on product distribution and rates of reactions.

During pulse experiments, the pattern and time scale at which different products exit from the reactor can provide indications of reaction pathways and primary/secondary products for each region. Figure 3 compare the product evolution during a single methane pulse injection in the first and the third region. While methane is mostly converted to CO_2 and H_2O in the first oxygen rich stage, dominant products in the third region are CO and H_2. The longer tail of the products in the third region also confirms stronger interaction between products and catalyst surface in this region.

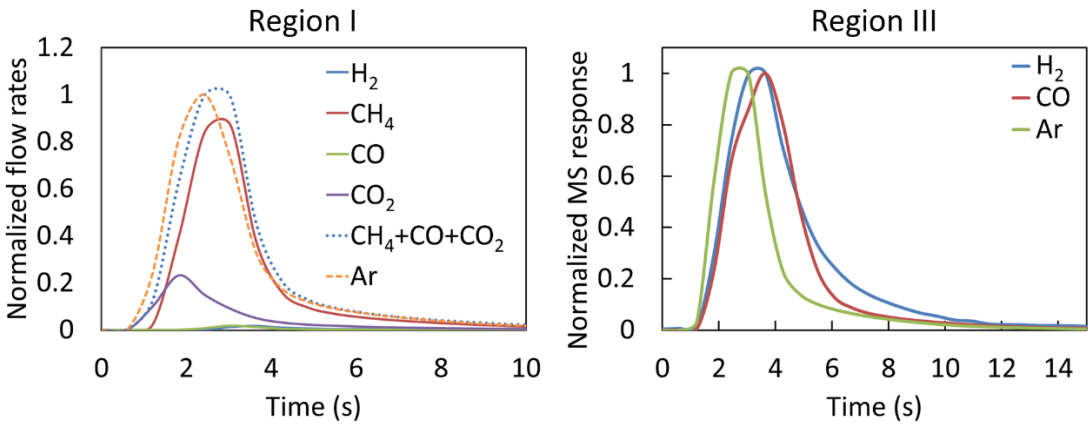

Figure 3. Product evolution during a single methane pulse injection in the first and the third region

To probe the role of methane adsorption/dissociation in regions i and iii, methane isotope exchange experiments are conducted through co-injection of CH_4 and CD_4. As can be seen in Figure 4, a very small amount of exchanged products are observed in the effluent gas at 900°C in the first region. This indicates i) low surface coverage of activated methane species and/or ii) facile oxidation of such species to CO_x products. Since the rate determining step is the oxidation reaction, which is controlled by oxygen conduction (methane dissociation and product desorption are not rate limiting from pulse experiments), the density of active sites for methane dissociation is concluded to be low. Moreover, such active sites are likely to be provided by surface oxygen species, which is affected by the rate of lattice oxygen conduction and evolution. In the third region, however, over 80% of the unreacted CH_4 and CD_4 in the third region exited the reactor as CH_3D, CH_2D_2, and CHD_3. This is conclusive evidence that methane dissociation in this region is significantly faster than its conversion, and that availability of surface oxygen controls the overall reaction rate.

Oxygen isotope exchange experiments are done by injection of $^{18}O_2$ pulse on $^{16}O_2$ treated catalyst. These experiments (Figure 4) confirmed that the surface of the catalyst in the first region is highly active for oxygen dissociation and exchange. In the third region, on the other hand, injected oxygens oxidized the reduced catalyst and no exchange is observed.

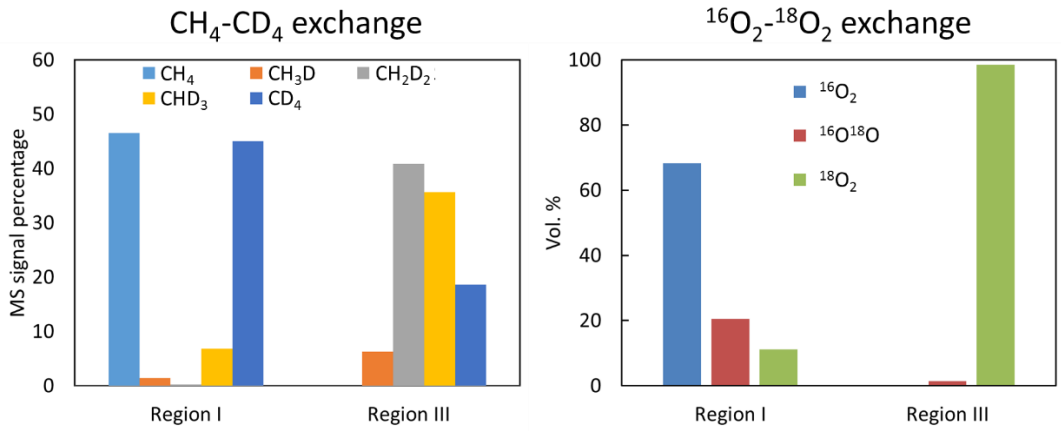

Figure 4. Methane and oxygen isotope exchange experiments on the redox catalyst

To probe the effect of lattice oxygen conduction, a redox catalyst sample is exposed to consecutive pulses of methane with varying relaxation times. Provided that oxygen conduction from the oxide lattice is a rate limiting step, longer relaxation time should allow increased amounts of bulk lattice oxygen being conducted to the surface and evolve into active oxygen species. This can, in turn, lead to increased methane conversion and decreased CO selectivity. As shown in Figure X, in the first region, selectivity of CO increased from 4.55% to 13.83% during the injection of 5 pulses with 15 seconds relaxation time; however, resting the sample for 2.5 minutes caused the selectivity to go down to 11.62%. The overall methane conversion also reduced from 43.7 µL in the first pulse to 22.2 µL in the fifth pulse and increased back up to 24.6 µL after longer relaxation. Similar behavior is observed in the third region. This

indicates that oxygen conduction is indeed rate-limiting in this region at 900°C and surface oxygen species are crucial for methane activation and oxidation.

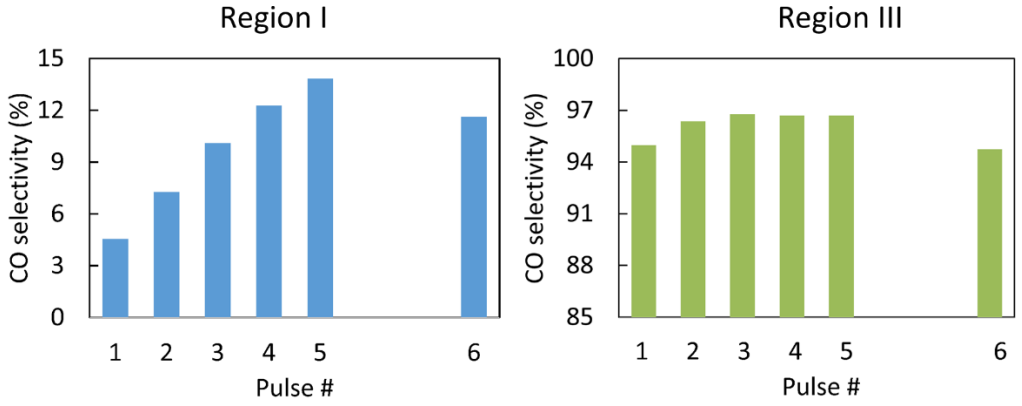

Figure 5. Effect of relaxation time on CO selectivity in the first and third region at 900°C (pulse 1-5 has a relation time of 15 seconds whereas pulses 5-6 has a longer relaxation time of 150 seconds).

These pieces of evidence suggest that while oxygen evolution maintains a modified Mars-van Krevlen mechanism throughout the reaction with O^{2-} conduction being the rate limiting step, the mechanism of methane conversion changes from an Eley-Rideal type in the first reaction region to a Langmuir-Hinshelwood-like mechanism in the third region. It is also concluded that abundance of surface oxygen species in the first region, which accounts for deep oxidation, makes the formation of oxygenated surface species dominant; whereas the lack of surface oxygen on the oxygen-deprived surface allows methane activation on metallic sites on the surface. Figure 6 schematically illustrates the mechanism change during the course of the metal oxide reduction reaction.

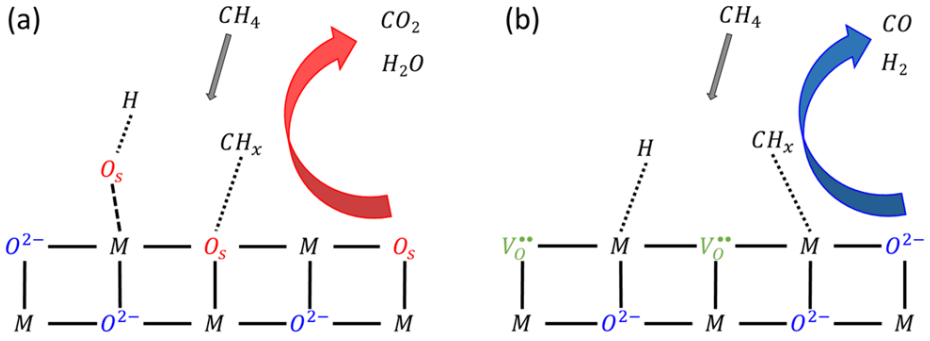

Figure 6. Schematics of methane activation and conversion of (a) oxidized and (b) reduced catalyst surface (M represents metal atoms).

Catalyst optimization

The aforementioned mechanistic findings indicate that higher syngas selectivity and lower coke formation can potentially be achieved by controlling the oxidation state of iron through partial redox cycles. Considering the effect of O^{2-} transport limitations and surface O^{2-} enrichment during the regeneration step, region i can be avoided by regenerating the iron oxide core to FeO whereas religion iv can be avoided by incomplete reduction of the catalyst. To validate the feasibility and potential advantages of partial redox cycles, a low concentration of steam (2% of flow) is added to the reaction gas to regulate the redox reactions. As shown in Figure 7, both region i and region iv are completely avoided under partial redox cycles. H_2 and CO productivity of 29.8 mmol/g and 9.4 mmol/g are achieved without coke formation. This corresponds to more than 100% increase in syngas productivity. Excluding hydrogen from steam, the overall syngas selectivity is estimated to be greater than 90%. The findings in the current study can help determine suitable reactor design and operating conditions for improved catalyst performance.

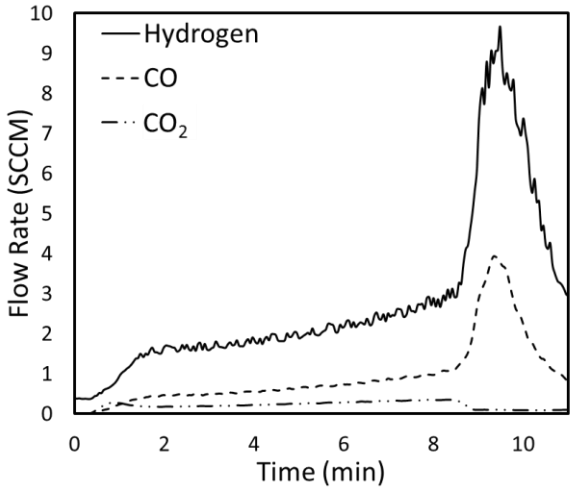

Figure 7. Reduction of partially regenerated core-shell catalyst in 20% methane 2% H_2O

Summary

Underlying mechanisms of methane partial oxidation over Fe_2O_3@LSF redox catalyst using a transient pulse injection method is investigated. The dynamic nature of reactions between methane and the redox catalyst introduces a four-region reduction scheme. In this study, a pulse injection system is used to inject sharp, transient pulses of various reactants in different sequences and concentrations to explore potential reaction pathways in different regions. The results indicate that the availability and nature of surface oxygen determines the reaction pathway and product selectivity. Oxygen anion conduction and/or its evolution to electrophilic surface oxygen species is determined to be the rate-limiting step in all the reduction regions of interest. Fe_2O_3@LSF redox catalyst goes through a mechanism change during the second region. While oxygen atoms maintain a modified Mars-van Krevlen mechanism throughout the reaction, the mechanism of methane conversion changes from the Eley-Rideal mechanism in the first region (in which methane is loosely adsorbed and reacts with electrophilic surface oxygen species) to a Langmuir-Hinshelwood-like mechanism in the third region (in

which dissociatively adsorbed CH_x species are partially oxidized by O^{2-} species on the surface). These findings indicate that redox catalysts that can inhibit the formation of non-selective surface oxygen species while maintaining a steady supply of lattice oxygen to the catalyst surface can potentially lead to improved performance for methane partial oxidation.

2. Perovskite promoted iron oxide for hybrid water-splitting and syngas generation with exceptional conversion

Low steam conversion in the water-splitting step of a thermal based water-splitting cycle will exert inevitable energy penalty on the process, since the second law dictates that latent heat in the steam-H_2 product mixture cannot be fully recuperated. A second law analysis indicates >3 kJ of exergy loss for every additional mole of unconverted steam. In practice, steam to hydrogen conversion for metallic iron and iron oxides is thermodynamically limited. For instance, at 930 °C, a maximum steam to hydrogen conversion of 62.3% is calculated by thermodynamic equilibrium of the FeO_x-H_2O-H_2 ternary system. Many of the iron containing redox materials exhibit even lower affinity to oxygen, leading to lower equilibrium constants for the water-splitting reaction (Reaction 1). Under the current project, we explore a highly effective, ferrite-based redox material for combined methane partial oxidation and water-splitting. Using perovskite-promoted iron oxide coupled with a layered reverse-flow reactor concept, over 77% steam to hydrogen conversion is achieved at 930 °C. The exceptional conversion, which is 15% higher than the maximum conversion predicted by the second law for iron (oxides), is achieved through synergistic effects between iron oxide and its perovskite support as well as a novel, layered reverse-flow reactor concept.

$MeO_{x-1} + H_2O \leftrightarrows MeO_x + H_2$ Reaction 1

To validate their high efficacy for water-splitting, iron oxides with 25% and 40% $La_{0.8}Sr_{0.2}FeO_{3-\delta}$ (LSF) support are prepared and tested in a fixed-bed reactor. The primary role of LSF support is to provide ionic and electronic conduction pathways for effective removal and replenishment of active lattice oxygen in iron oxides. Such an effect has been confirmed through our recent studies.[2–5] A reduced iron phase is first created by contacting the redox material with hydrogen or CO. H_2 is used as reducing gas to rule out coke formation and its subsequent contribution towards H_2 generation through steam-carbon reaction. When re-oxidized, steam to H_2 conversion of these perovskite-supported redox materials (64±0.7% and 67±1.3%) as shown in Figure 8 are consistently higher than those predicted by the FeO_x-H_2O-H_2 equilibrium (62.3%) at 930 °C. Excellent stability is also achieved over multiple redox cycles. Similar steam conversions are observed for redox materials reduced with CO. The exceptional steam conversion with LSF-supported iron oxide, which is higher than the nominal thermodynamic limit of 62.3%, is certainly not unphysical. Rather, it can be explained by the high oxygen affinity of LSF precursors as well as the oxygen vacancies in reduced LSF.

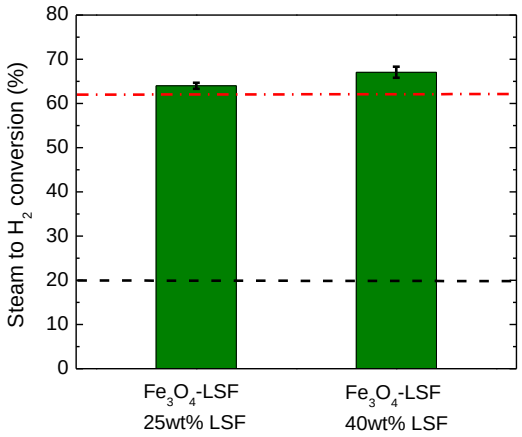

Figure 8. Average steam conversion (%) of Fe_3O_4-LSF in the oxidation step at 930 °C (regenerated to an average composition of $FeO_{0.5}$). Error bars indicate 95% confidence interval for steam conversion form multi-cycle experiments (see ESI). Red dash-dotted line shows the maximum steam conversion for FeO_x-H_2O-H_2 ternary system based on thermodynamic equilibrium. Black dashed line shows the highest literature-reported steam conversion.[6–11]

In order to reveal the contribution of LSF to the overall water-splitting reaction, steam oxidation of reduced LSF-Fe_2O_3 is conducted in a thermal gravimetric analyzer (TGA). A H_2-steam mixture with decreasing H_2 concentrations is introduced into the TGA, and the sample weight change is recorded. Weight gain of the sample under a specific H_2 concentration, defined as $F_{H2}\ (F_{H2}+F_{H2O})^{-1}$, indicates that the sample is capable of achieving the corresponding or higher steam to H_2 conversion. In Figure 9A, four regions are found under varying H_2 concentrations. The corresponding phases are analyzed by X-ray powder diffraction (XRD) (Figure 9B). The reduced redox material is primarily composed of a composite of Fe, La_2O_3, and a very small amount of $LaSrFeO_{4-\delta}$. These reduced metallic iron and oxide species are stable under 100% H_2 (Region I). However, they are easily oxidizable even in the presence 95% H_2 balanced steam (P_{O2}=5×10^{-19} atm at 930 °C). Such a high affinity to oxygen is not observed in a pure Fe-O system, as iron is only oxidized to wüstite at P_{O2} = 6×10^{-17} atm or higher (equivalent to 62.3% steam conversion). The main driving force for the exceptional steam conversion, as evidenced by XRD spectra of the partially oxidized sample in Region II, is the solid state reaction among iron, La_2O_3, and SrO in the presence of water as well as water-splitting reaction of defected LSF. Such reactions can be generalized as:

$$La_{0.8}Sr_{0.2}FeO_{3-\delta'} + (\delta' - \delta)\ H_2O \leftrightarrow La_{0.8}Sr_{0.2}FeO_{3-\delta} + (\delta' - \delta)\ H_2 \qquad \text{Reaction 2}$$

where $0 \le \delta < \delta' \le 1.6$. The specific reaction involved in Region II is:

$$0.4La_2O_3 + 0.2SrO + Fe + (1.6 - \delta)\ H_2O \leftrightarrow La_{0.8}Sr_{0.2}FeO_{3-\delta} + (1.6 - \delta)\ H_2 \qquad \text{Reaction 3}$$

Reaction 3 can be considered as a special case of Reaction 2, under which the oxygen defect concentration is too large to maintain a stable perovskite structure. The contribution of Reactions 2 and 3 to overall water-splitting reaction can be determined based on defect formation energies in LSF

perovskites, which can accommodate significant oxygen non-stoichiometry resulting from acceptor (Sr) doping in its A-site cations and the variable valence states of its B-site (Fe) cations.[12] Using the defect model proposed by Mizusaki and Murugan et al[13–15], the relationship between oxygen vacancy (δ) and oxygen partial pressure is determined by:

$$\frac{\delta^{\frac{1}{2}}(2\delta - x + 1)}{(3-\delta)^{\frac{1}{2}}(2\delta - x)} p_{o_2}^{\frac{1}{4}} = \frac{K_{Fe}}{K_{Ox}} \frac{(1 + x - 2\delta)(3-\delta)^{\frac{1}{2}}}{\delta^{\frac{1}{2}}(2\delta - x)} \frac{1}{p_{o_2}^{\frac{1}{4}}} - \frac{1}{K_{Ox}^{\frac{1}{2}}} \qquad \text{Equation 1}$$

where x = 0.2 for $La_{0.8}Sr_{0.2}FeO_{3-\delta}$. Since the above model is suited for defected perovskites with very high steam conversions, it can accurately estimate steam conversions in both Reaction 2 and 3. As shown in Figure 9A, the model predictions are in good agreement with TGA results. The slight over-prediction in Region II and III is partly due to incomplete reduction of the sample prior to steam oxidation, as confirmed by XRD in Figure 9B.

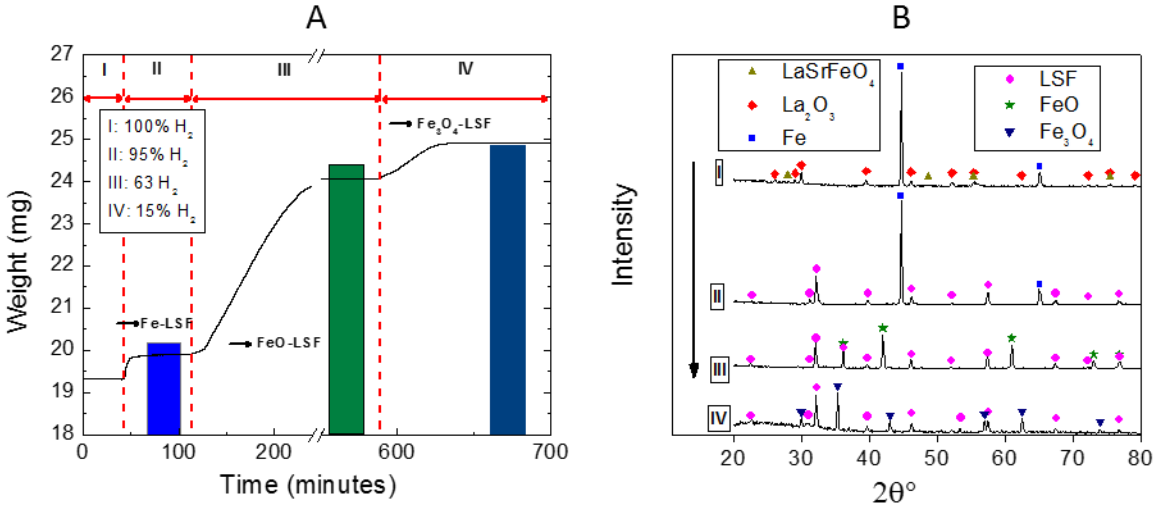

Figure 9. (A) TGA profile of the reduced Fe_3O_4-LSF particle oxidized by steam and hydrogen mixture at 930°C. (I) in the presence of pure H_2; (II) oxidized by 95% H_2 (balance steam,N_2-free basis); (II) oxidized by 63% H_2; (IV) oxidized by 15% H_2. (B) XRD results of the particles when weight is stabilized in regimes (I), (II), (III) and (IV).

In the subsequent oxidation step in Region III, the main oxygen acceptor for water-splitting is metallic iron, forming wüstite. Oxygen vacancies in the LSF phase also contribute to a small fraction of the oxygen uptake. The corresponding steam to H_2 conversion in such a step is shown to be around 63%, which is in-line with equilibrium steam conversion between Fe to FeO (62.3%). As confirmed via TGA, iron (oxide), through phase transition from iron to wüstite, is responsible for 85.8% of the hydrogen generated from water-splitting with the LSF phase contributing the remaining 14.2%. The contribution from the LSF phase, albeit small, is essential for steam conversion (Figure 10A). Based on the defect model, theoretical steam conversion for 25 wt% LSF promoted iron oxide is predicted to be 65.7% assuming iron and LSF phases act independently for water-splitting (additive effect). Besides the

abovementioned additive effect, which is appropriate to describe composite LSF-iron oxide redox catalysts in a conventional fixed bed, one can also envision a scenario under which steam reacts with reduced iron (oxide) and LSF in a sequential manner. Such a configuration puts steam in sequential contact with two redox materials with increasing oxygen affinity (or water-splitting efficacy). As a result, the overall thermodynamic driving force for water-splitting is maximized. As illustrated in Figure 10B, further improvement in steam conversion can be anticipated under the sequential case.

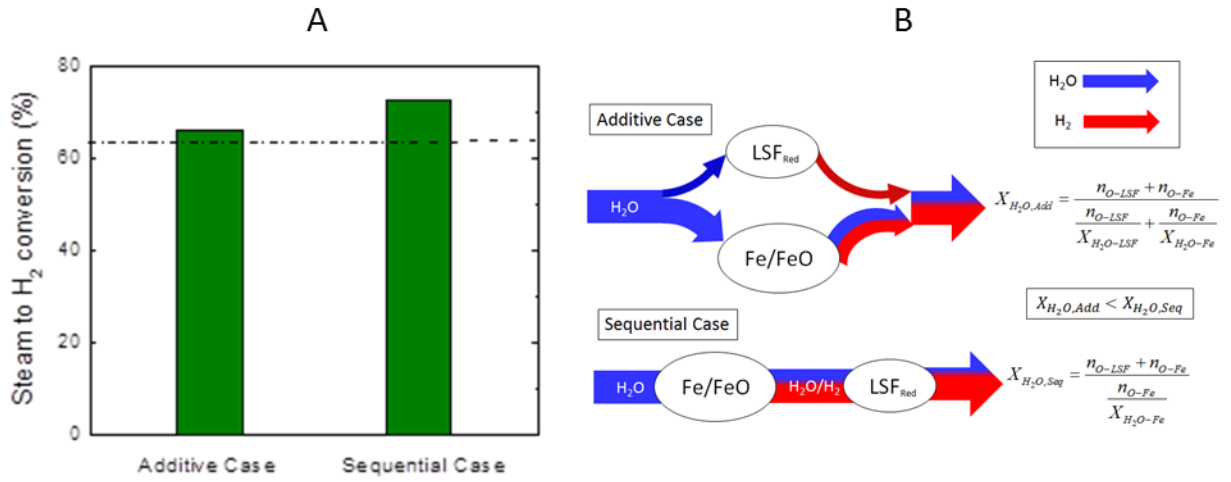

Figure 10. (A) Equilibrium steam conversion calculated based on an additive effect and sequential effect for iron oxide promoted with 25wt% LSF at 930 °C; (B) Schematic illustration of the additive and sequential cases. $n_{O\text{-}Fe}$ and $n_{O\text{-}LSF}$ represent the oxygen uptake by reduced iron oxide and LSF during water-splitting. $X_{O\text{-}Fe}$ and $X_{O\text{-}LSF}$ are equilibrium steam conversions for reduced iron oxide and LSF. $X_{H2O,Add}$ and $X_{H2O,Seq}$ refer to overall steam conversion in additive case and sequential case (equations shown are generally applicable to redox catalysts with <50 wt% LSF).

In order to achieve the perceived advantage of the sequential reaction scheme, a layered reverse-flow reactor design using Fe_3O_4-LSF is proposed for combined syngas generation and water-splitting. As illustrated in Figure 11, the reactor is composed of two layers. The bottom layer is iron (oxide) rich, whereas the top layer is primarily composed of LSF. A small amount of LSF at the bottom layer is necessary to prevent iron oxide sintering and deactivation. During the syngas generation stage, methane is introduced from the top of the reactor, producing syngas while removing the active lattice oxygen from both LSF and iron oxide-LSF layers. Since LSF has higher resistance towards coke formation,[4] injecting methane from the LSF end would be advantageous. Upon completion of the reduction reaction, steam is introduced from the bottom of the reactor to react with the reduced iron oxide-LSF layer and then the LSF layer. Such an arrangement maximizes the thermodynamic driving force for water-splitting while taking advantage of the unique properties of LSF for methane partial oxidation. As a result, high syngas yield and exceptional steam conversion can be achieved. The concept illustrated in Figure 11 can be extended to general cases where concentration gradients of LSF and iron oxide are created along axial position of the fixed bed reactor.

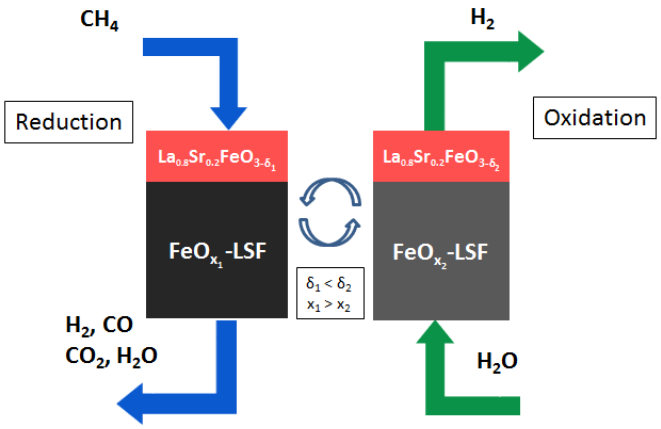

Figure 11. Schematic of the proposed layered reverse-flow redox process with exceptional steam conversion and syngas yield.

Summary

In summary, LSF-promoted iron oxide is demonstrated to be an exceptional redox material in a hybrid redox scheme for methane partial oxidation and water-splitting. Coupled with a novel layered reverse-flow reactor concept, the redox material is shown to be capable of converting over 77.2% steam into hydrogen. Such a conversion not only triples the performance of existing thermochemical based water-splitting processes, but also significantly exceeds the theoretical water-splitting efficiency for unpromoted iron oxides. When applied to the hybrid solar-redox scheme for liquid fuel and hydrogen co-generation, the process efficiency can increase by 15.1% (HHV) and CO_2 emission for H_2 product is reduced by up to 60%.

3. Investigation of lower cost perovskite MIEC materials

Synthesis of composite oxides

Three perovskite-supported ferrites are prepared along with a reference, YSZ supported oxygen carrier. The compositions of these single-phase and composite oxides are summarized in the table below. Fe_2O_3–LSF composites are investigated because our previous studies confirmed high redox activity of a similar oxygen carrying material.[2,3,5] BCF and CTF perovskites are selected due to their varying ionic and electronic conductivities. Solid state reaction (SSR) is used to synthesize the oxides. This methods allows the formation of a mixed matrix between the (primary) iron oxide and perovskite support. Such a composite structure is similar to most oxygen carriers reported in literature. YSZ, a frequently used support and an ionic conductor, is used as the support for the reference oxygen carrier. Details of the synthesis methods are presented in the previous report.

Sample No.	Composition (w.t.%)	Preparation Method

LSF-1	50% Fe_2O_3, 50% $La_{0.7}Sr_{0.3}FeO_3$	Solid State reaction
BCF-1	50% Fe_2O_3, 50% $BaCe_{0.7}Fe_{0.3}O_3$	Solid State reaction
CTF-1	50% Fe_2O_3, 50% $CaTi_{0.85}Fe_{0.15}O_3$	Solid State reaction

Sample characterization and redox testing

Various characterization techniques are used to analyze the structural, surface, and morphological properties of the oxide samples. The crystalline phases present in each sample before and after redox tests are analyzed by X-ray powder diffraction (XRD). The specific surface areas of the samples are measured with a BET surface analyzer and Scanning electron microscopy is used to observe the morphologies of the samples.

All reactivity studies are conducted in a differential bed reactor system composed of a computer controlled panel for gas mixing and delivery, a thermal gravimetric analyzer for redox reactions. Cyclic studies, including 5 and 50-cycle redox cycles, are conducted to determine the short term and long-term stability and reactivity of the oxygen carriers, respectively.

Redox activity study

Reaction rates of perovskite and YSZ supported composite oxides with 10% H_2 are compared using three quantitative parameters, including the time to reach 11% conversion, the time to reach 33% conversion and the time to reach 80% conversion, which correspond to iron oxide reduction to Fe_3O_4, FeO, and (70 mol.%) Fe–FeO mixture, respectively. Longer reduction time generally corresponds to lower activity. These parameters for the four samples at their 2nd reduction cycle are shown in Figure 12. As can be seen, activities of the three perovskite supported composite oxides are as follows: CTF-1 < BCF-1 < LSF-1. It is noted that mixed-conductivities of the three mixed-conductors follow the same trend of CTF < BCF < LSF.[16] When compared with YSZ supported composite oxide with comparable surface area of 0.57 m^2 /g, perovskite supported samples exhibit significantly higher activity. This is consistent with the low electronic conductivity (or electronic transference number) of YSZ. The lack of electronic conductivity of YSZ inhibits the conduction of O_2 since local charge needs to be balanced. To summarize, mixed ionic–electronic conductivity of support directly correlates to oxygen carrier redox activity, i.e. supports with higher mixed conductivity lead to improved redox activity.

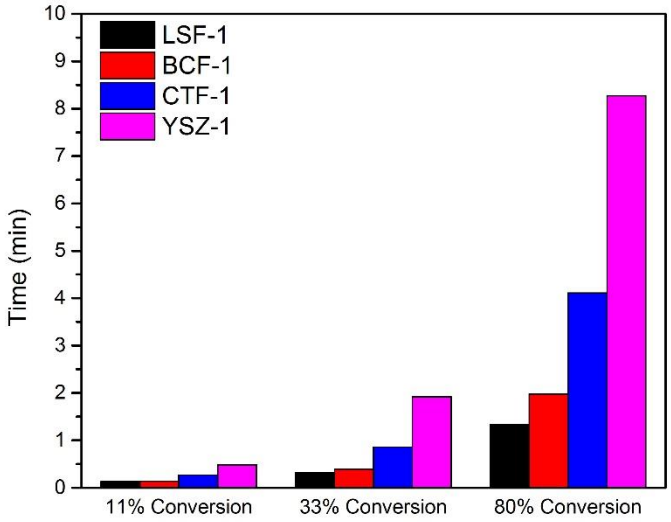

Figure 12. Effect of perovskite support on reactivity of composite oxides. Reducing gas: 10% H2; Temperature: 900 °C.

Summary

This part of the study investigates the redox performance of several mixed-conductive perovskites, i.e. LSF, BCF and CTF, both as supports and standalone oxygen carriers. Their redox performances are compared to oxygen carriers prepared with a reference YSZ support. Among the three perovskites, CTF synthesized via a solid-state reaction method exhibits the highest stability under a reducing environment. Redox activity of the oxygen carrier is found to correlate with mixed-conductivity of the support. Although CTF is less conductive than BCF and LSF, CTF supported iron oxide exhibits satisfactory redox activity compared to the reference oxygen carrier. Further investigations indicate that the initial activity of CTF supported oxygen carrier is not correlated with its surface area. Besides mixed-conductivity of the support, O_2 transfer within iron oxide particles can be important at the final stage of the reduction. This is confirmed by incomplete reduction of CTF supported iron oxide when larger iron oxide precursor particles are used. Studies on ionic diffusions between CTF support and iron further confirms that the mixed-conductive support assists the lattice oxygen exchange between iron (oxides) and gaseous reactants. Therefore, CTF, which is prepared from earth-abundant precursors, can function as an effective mixed-conductive support for iron oxide based oxygen carriers. Multi-cyclic studies indicate that CTF supported iron oxide is both stable and active through extended redox cycles. Further improvements in oxygen carrier activity can potentially be achieved by enhancing support mixed-conductivity and reducing iron oxide particle sizes.

Conclusion

To sum up, the support from ARO has allowed us to investigate the effect of support, mechanism, and novel applications of perovskite supported iron oxide as a versatile redox catalyst. Properly designed redox catalyst are shown to be highly effective for syngas partial oxidation and water-splitting. In addition, coke formation can be avoided if the redox catalyst is regenerated before complete reduction of iron oxide into metallic iron. High syngas selectivity, steam to hydrogen conversion, and inhibition of coke formation are observed in the current study. Further studies to understand details of solid state oxygen anion conduction, dopant effect, and redox catalyst optimizations are highly desirable.

Outcome from the ARO Support

The ARO support and the related redox catalyst studies have resulted in the following scholarly products:

Neal, L. M., Shafiefarhood, A. & Li, F. *Dynamic Methane Partial Oxidation Using a Fe_2O_3@$La_{0.8}Sr_{0.2}FeO_{3-\delta}$ Core–Shell Redox Catalyst in the Absence of Gaseous Oxygen*. ACS Catal. 4, 3560–3569 (2014).

Chen, Y., Galinsky, N., Wang, Z. & Li, F. *Investigation of perovskite supported composite oxides for chemical looping conversion of syngas*. Fuel 134, 521–530 (2014).

He, F. & Li, F. *Hydrogen production from methane and solar energy – Process evaluations and comparison studies*. Int. J. Hydrog. Energy 39, 18092–18102 (2014).

He, F. & Li, F. *Perovskite promoted iron oxide for hybrid water-splitting and syngas generation with exceptional conversion*. Energy Environ. Sci. 8, 535–539 (2015).

Shafiefarhood, A., Hamill, J. C., Neal, L. M. & Li, F. *Methane partial oxidation using FeO_x@$La_{0.8}Sr_{0.2}FeO_{3-\delta}$ core–shell catalyst – transient pulse studies*. Phys. Chem. Chem. Phys. 17, 31297–31307 (2015).

Bibliography

1. Shafiefarhood, A., Galinsky, N., Huang, Y., Chen, Y. & Li, F. Fe2O3@LaxSr1−xFeO3 Core–Shell Redox Catalyst for Methane Partial Oxidation. *ChemCatChem* **6,** 790–799 (2014).
2. Galinsky, N. L., Huang, Y., Shafiefarhood, A. & Li, F. Iron Oxide with Facilitated O2– Transport for Facile Fuel Oxidation and CO2 Capture in a Chemical Looping Scheme. *ACS Sustain. Chem. Eng.* **1,** 364–373 (2013).
3. Shafiefarhood, A., Galinsky, N., Huang, Y., Chen, Y. & Li, F. Fe2O3@LaxSr1−xFeO3 Core–Shell Redox Catalyst for Methane Partial Oxidation. *ChemCatChem* **6,** 790–799 (2014).
4. Neal, L. M., Shafiefarhood, A. & Li, F. Dynamic Methane Partial Oxidation Using a Fe2O3@La0.8Sr0.2FeO3-δ Core–Shell Redox Catalyst in the Absence of Gaseous Oxygen. *ACS Catal.* **10,** 3560–3569 (2014).

5. He, F., Trainham, J., Parsons, G., Newman, J. S. & Li, F. A hybrid solar-redox scheme for liquid fuel and hydrogen coproduction. *Energy Environ. Sci.* **7,** 2033–2042 (2014).
6. Go, K. S., Son, S. R., Kim, S. D., Kang, K. S. & Park, C. S. Hydrogen production from two-step steam methane reforming in a fluidized bed reactor. *Int. J. Hydrog. Energy* **34,** 1301–1309 (2009).
7. Yamaguchi, D. *et al.* Hydrogen production through methane–steam cyclic redox processes with iron-based metal oxides. *Int. J. Hydrog. Energy* **36,** 6646–6656 (2011).
8. Kidambi, P. R., Cleeton, J. P. E., Scott, S. A., Dennis, J. S. & Bohn, C. D. Interaction of Iron Oxide with Alumina in a Composite Oxygen Carrier during the Production of Hydrogen by Chemical Looping. *Energy Fuels* **26,** 603–617 (2012).
9. Kierzkowska, A. M. *et al.* Development of Iron Oxide Carriers for Chemical Looping Combustion Using Sol−Gel. *Ind. Eng. Chem. Res.* **49,** 5383–5391 (2010).
10. Rydén, M. & Arjmand, M. Continuous hydrogen production via the steam–iron reaction by chemical looping in a circulating fluidized-bed reactor. *Int. J. Hydrog. Energy* **37,** 4843–4854 (2012).
11. Galvita, V., Hempel, T., Lorenz, H., Rihko-Struckmann, L. K. & Sundmacher, K. Deactivation of Modified Iron Oxide Materials in the Cyclic Water Gas Shift Process for CO-Free Hydrogen Production. *Ind. Eng. Chem. Res.* **47,** 303–310 (2008).
12. Peña, M. A. & Fierro, J. L. G. Chemical Structures and Performance of Perovskite Oxides. *Chem. Rev.* **101,** 1981–2018 (2001).
13. Mizusaki, J., Sasamoto, T., Cannon, W. R. & Bowen, H. K. Electronic Conductivity, Seebeck Coefficient, and Defect Structure of La1-xSrxFeO3 (x=0.l, 0.25). *J. Am. Ceram. Soc.* **66,** 247–252 (1983).
14. Mizusaki, J., Yoshihiro, M., Yamauchi, S. & Fueki, K. Nonstoichiometry and defect structure of the perovskite-type oxides La1−xSrxFeO3−°. *J. Solid State Chem.* **58,** 257–266 (1985).
15. Murugan, A., Thursfield, A. & Metcalfe, I. S. A chemical looping process for hydrogen production using iron-containing perovskites. *Energy Environ. Sci.* **4,** 4639–4649 (2011).
16. Sunarso, J. *et al.* Mixed ionic–electronic conducting (MIEC) ceramic-based membranes for oxygen separation. *J. Membr. Sci.* **320,** 13–41 (2008).